

The Composite Luminosity Function of A496 [★]

Emilio Molinari¹, Guido Chincarini^{1,2}, Alberto Moretti¹, Sabrina De Grandi¹

¹ Osservatorio Astronomico di Brera, via Bianchi 46, I-23807 Merate (LC), Italy

² Università degli Studi, via Celoria 16, Milano, Italy

e-mail to: molinari@merate.mi.astro.it

Accepted ...; Received ...

Abstract. Deep photometric observations in three colours of the cluster A 496 show that the luminosity function is bimodal with a deep gap at $g \sim 19.0$. That is there is a net separation between E/SO galaxies that are nicely fitted by a gaussian distribution curve and the dwarfs that better match a Schechter Function. This is the first cluster observed and reduced out of a sample of 19 clusters which we have in our program. However comparison with the data of Virgo and Coma might suggest a correlation between cluster morphology and amplitude of the two distribution: Normal and dwarf population. This would have strong implication for the understanding of cluster formation and evolution so that we are pursuing the estimate of the LF in various colours and to faint magnitudes both for low and high redshift clusters.

Key words: galaxies: clusters: general - galaxies: luminosity function - galaxies: photometry

1. INTRODUCTION

A break through in the cluster galaxies luminosity function came with the operation of the Du Pont Telescope and the observations carried out by Sandage and collaborators on the Virgo gluster of galaxies (see Bingeli et al. 1988 for a review).

The Virgo cluster is a rather poor cluster and showed that the luminosity of normal galaxies follows a gaussian distribution while dwarfs galaxies tend to follow a Schechter distribution function. The envelope of the distributions, that is the composite luminosity function of the mix of morphological types, is again quite well represented by a Schechter Function. There is no discontinuity between the domain of the normal and dwarfs galaxies. Since the faint end has very strong implication on the cluster mass to luminosity ratio and its comparison to the

[★] Based on observations made at the European Southern Observatory (ESO), La Silla, Chile

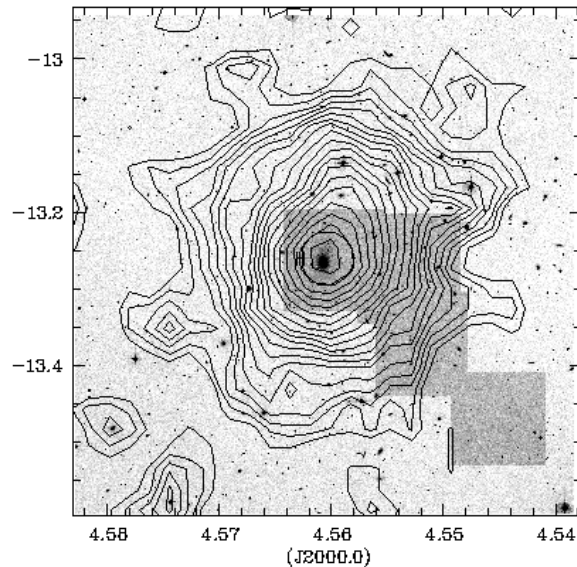


Fig. 1. Abell 496 clusters of galaxies image extracted from the POSS digital plates. The X-ray Rosat all-sky survey contours have been overplotted in arbitrary units. The circle near the center is the core radius of the X-ray emission and the shaded area represents the observed fields in this work. The coordinates refer to the J2000 ephemerides.

non cluster galaxies give important insights into the cluster formation and evolution, we decided, 1994, to observe the luminosity function of a subsample of clusters detected by the ROSAT all-sky survey (De Grandi, 1996). The subsample covers the Bautz-Morgan morphological types I, I-II and II and will enable us to estimate properties as a function of the optical and X-ray cluster morphology. Details of the sample selection, properties of the clusters and a description of the data reduction and analysis procedure will be given in Moretti et al (1998). Our study was also motivated by the finding, Marzke et al. 1994, that the non cluster galaxies luminosity function raises consid-

erably at faint magnitudes. The comparison cluster non-cluster galaxies became mandatory.

After our program started Bernstein et al. (1995) published their very deep observations of the central part of the Coma Cluster. These observations are a milestone regarding the faint end of the luminosity function where we want to disentangle the dwarfs and spheroidal galaxies population from the globular clusters. This in order to fully understand the formation and evolution of that population. These authors, however, do not have enough accuracy and statistics on the bright end in order to determine accurately the luminosity function. Biviano et al. (1995), on the other hand, using a very clean (low back-for-ground contamination) spectroscopically selected sample of galaxies in the Coma Cluster show that the luminosity function of that cluster is bimodal. They notice a lack of galaxies at about $b \sim 17.5$ and that is the separation between normal and dwarf E/SO. Lopez & Yee (1996) and Molinari & Smareglia (1998) stress that the composite nature of the luminosity function could be a function of morphology and age given the variation of the galaxy mix as a function of type. Indeed the fact that the composite (without morphological type selection) luminosity function in Coma shows a discontinuity while that is unnoticeable in the Virgo Cluster might call for a strong correlation with cluster morphology. The claim of an universal form for the cluster luminosity function (Colless 1989) might come to an end, though it had appealing connections with a standard fragmentation scenario for structure formation (see, however, Trentham 1997 and 1998, which find a similar LF both in clusters and in the field).

We think however that the new findings which we describe here (on line with the work of Biviano et al. 1995) shed new light on the mechanism of cluster formation and evolution.

2. THE DATA

In this first paper we estimate the population content of the cluster A 496 and measure the luminosity function in three passbands. Abell 496 is a cD dominated cluster with a very regular, spherical X-ray emission. The hot gas extension reaches, in the Rosat all-sky survey, 15-20 arcmin from the center. Fig. 1 shows the X-ray contours over the digitized POSS image. The gray area has been imaged in the Dec. 94 run.

The cluster of galaxies A496 is at a redshift $z=0.0320$. The distance modulus of the cluster is $m_r - M_r = 36.42$ adopting $H_0 = 50\text{km/sec/Mpc}$ and a k -correction of 0.01 mag. To image the cluster we used the DFOSC camera at the Cassegrain Focus of the ESO-Danish 1.5 m telescope. In order to sample the cluster at a rather large distance from the cluster center and minimize the observing time, we observed a mosaic area composed of 4 fields along a radial direction and each extended $8.68 \times 8.68 \text{ arcmin}^2$. The total area observed amounts, accounting for some overlap-

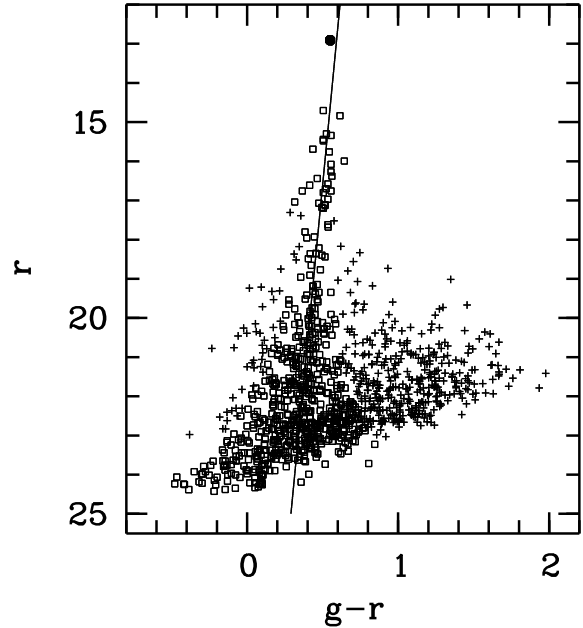


Fig. 2. The colour-magnitude plot for the 1058 non star objects for which we have g and r magnitudes. The cD galaxy is represented by the larger symbol in the upper part of the plot. The bright E/SO galaxies, open squares above $r \sim 18$, fix the solid line drawn in the middle of the plot and define the c-m sequence for elliptical galaxies. The population of fiducial early type galaxies which lie on the c-m sequence is plotted also as open squares (see beginning of section 3). The distribution of points clearly shows the effect due to the limiting magnitude in the various colours. Note in addition that below the horizontal line of $r = 20.75$ there is a 10%-15% contamination due to galactic stars.

ping, to about 225 arcmin^2 . Each field has been observed in the colour g , r and i defined by the Gunn filters. The centers of the effective transmission, which is inclusive of telescope and camera response, are at 4930, 6500 and 8200 Å. The integration lasted 1 hour per field with a typical seeing of 1.2 arcsec FWHM estimated on the stacked images. A pixel size of 0.5 is good enough to stack the shift and stare images as to fully use of the strategy used to gain flat field smoothness and ease cosmic rays removal.

Overlapping of different fields allowed us to determine the internal consistency of photometry. We estimated a 1-sigma error at magnitude 22 of 0.20, 0.19 and 0.22 mag in the g , r and i filters respectively. The overall errors are dominated by the poissonian counting noise.

We estimated the effect of crowding in the detection of objects by the search algorithm that we used (package INVENTORY, see West & Kruszewski, 1981) by simulation. Simulated galaxies (extracted by the same CCD images of our sample) of different magnitudes were added randomly to the images we were measuring and the search process for objects was repeated various times. The result is a re-

lation which estimates the probability of detection as a function of magnitude and position in the field of view: the major source of incompleteness still remains the background fluctuation, which affects in a different way the central cD dominated area. Full details on the $p(m, R)$, where m is the magnitude and R the distance from the cD centre will be given in Moretti et al (1998). We measured that we had still an efficiency as high as 50% down to $r \sim 24.5$ all over the field but in the central region. The higher central background light due to the cD galaxy prevented us to detect objects fainter than $r \sim 23$. The area involved is nevertheless limited and the cD halo action in hiding faint objects starts its efficiency at $r > 23$. Part of the problem of the detection of faint objects in the presence of a bright background due to the halo of bright galaxies was overcome by modelling the shape of the giant galaxies and removing them from the frames to be measured. Details on the complete data reduction procedures will be given by Moretti et al. (1998) in conjunction with the whole photometric catalogue.

Up to $r \sim 20.5$ we were able to distinguish easily stars from galaxies using the isophotal radius. Fainter objects were however seeing limited so that a safe estimate based on the PSF was not possible. We thus decided to keep in a conservative way all the faint objects in our working catalogue. An analysis of the galactic stellar contamination (Robin et al. 1995) yielded a number of ~ 300 stars with magnitude $20.75 < r < 24.4$, or about 15% of our objects. Restricting the analysis where the sequence of early type populates the c-m plane (see Fig. 2) the level of contamination is even lower (less than 10%). All this taken into account, from the complete photometric catalogue of 2355 objects a set of 279 identified stars with $r < 20.75$ are removed. The remaining 2076 objects, with at least one filter measured, suffer from contamination between $r = 20.75$ and the limiting magnitude of $r \sim 24.5$ from the presence of a 10%-15% of galactic stars. As the stars are rather few, the results of the analysis about the luminosity functions should not be altered by such low contamination. In the case of correction by subtraction the star contribution is statistically cancelled, and the study of the E/S0 population (see Section 4.1) is affected by a even lower star fraction.

We were able to measure g magnitudes for 1080 galaxies, r for 2054 and i for 1499: 1058 galaxies have both g and r magnitudes and 955 g , r and i . The limiting magnitudes (50% efficiency in detection) are 24.14, 24.46, 23.75 for g , r and i respectively. All the magnitudes used in this work are isophotal magnitudes, computed integrating the flux within an isophote of 2σ the sky noise in each filter. For ease of comparison with other magnitude definition we have undergone the whole photometric measurement for a set of objects with known *true* flux, obtained scaling down to faint brightness a bright, non saturated object (much like as used in the incompleteness analysis). Our isophotal magnitude does not differ significantly up to $r \sim 23.5$

for stellar like objects from the known magnitude. For an elliptical galaxy surface brightness distribution the error, in the sense of our magnitude look fainter, is as much as 0.47 mag when the *true* one is 22. Somewhat higher differences are expected for disk like and irregular galaxies. In our subsequent analysis we have not performed any correction and used Inventory isophotal magnitudes.

3. THE CLUSTER POPULATION

As expected for a cD cluster, early type galaxies dominate the central region and these are easily identified by visual inspection down to $r \sim 18$. By using this set of bona fide early type galaxies we can compute the best fit of the linear sequence they define in the $g-r / r$ plane and extrapolate it to fainter magnitudes. The linear sequence of early type galaxies is, indeed, well defined down to $r \sim 21.5$ with an intrinsic spread about the mean of $(g-r) \sim 0.2$ mag at $r \sim 21$. The presence of a distinct population which obeys a colour-magnitude relation allowed different author to single out the early type population belonging to a cluster (among the others Metcalfe et al. 1994, Secker 1996 for rich clusters, Molinari and Smareglia 1998 using a neural network to exploit multi-colours information and De Propris and Pritchett 1998 who extend the c-m down to the faint magnitude of $M_I \sim -14$). We thus decide to partition the whole set into three classes: the fiducial early type, lying in the region of the r vs. $g-r$ plane closer to the c-m relation less than 1σ of the poissonian error of our photometry (i.e. $|(g-r) - cm_{E/S0}| \leq 0.28 \times 10^{0.2(r-22)}$); the red objects, with $g-r$ colour greater than ~ 0.8 ; the objects bluer than $g-r \sim 0$. In Fig. 2 we mark with different symbols the early type galaxies that belong to the linear sequence we mentioned and the bluer and redder objects which define different populations.

3.1. The red and the blue objects

The two extreme populations, i.e. the reddest and bluer objects which lie apart from the early type c-m relation, deserve at least a brief attention.

The red objects can be viewed in their spatial distribution in Fig. 3 (upper panel), showing no clear sign of clumpiness. The random distribution is evidenced also in the $g-r$ vs. $g-i$ phase space: the presence of a fore- or background cluster would have shown up as a overdensity of points at a particular colour location. Using a population synthesis model (Buzzoni 1995, the solid line in Fig. 3, lower panel) we can follow the expected colour shift as a function of redshift predicting the effect of a purely passive evolutionary k -correction. The points in the plane clearly stretch from bluer (zero redshift) to redder colours, spreading out to a redshift $z \sim 0.8$. We are therefore lead to the classification of these objects as background (mainly E/S0) galaxies. Some of the points, anyway, are probable galactic stars, especially in the upper, bluer $g-i$, strip

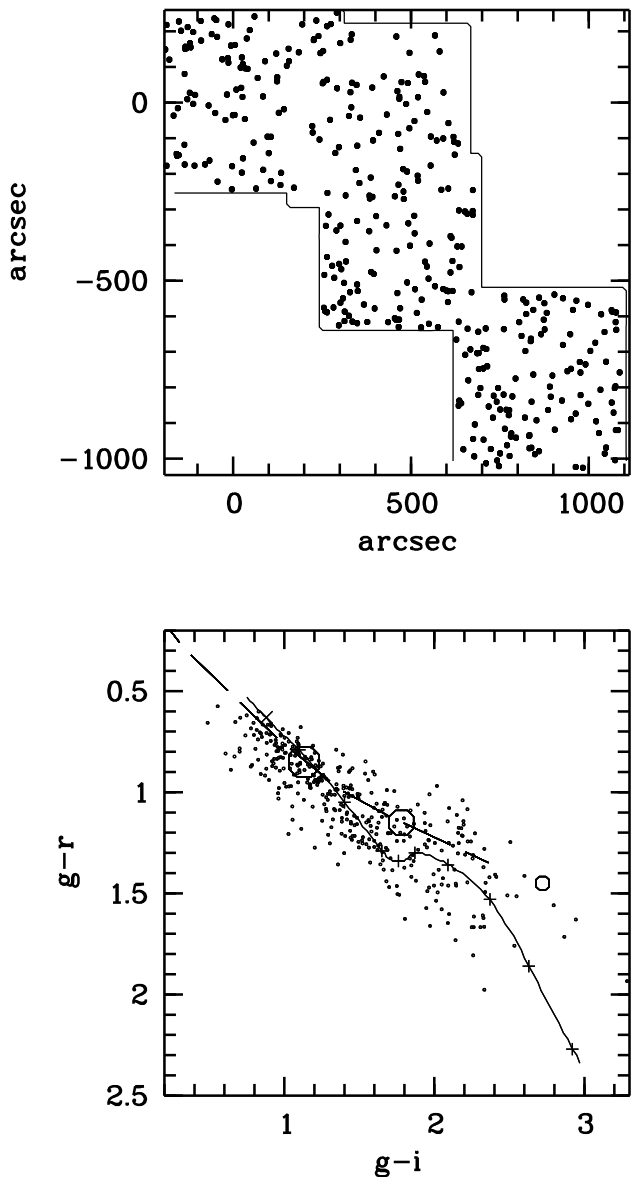


Fig. 3. Distribution of the redder objects as described in the text. The upper plot shows the distribution on the sky: this is quite uniform without any evidence of clustering. In the bottom panel the same objects have been plotted in the colour-colour plane, $g-r$ versus $g-i$. All the points are spread, without any particular clustering, over the line indicating the position of elliptical galaxies as a function of redshift: the crosses are separated by a difference of 0.1 in redshift starting from $z = 0$ (upper left) to $z = 1$ (bottom right). The scarcity of points going toward the red is expected in a sample limited in magnitude. In the upper plot the origin has been taken at the position of the cD galaxy while the evolutionary sequence in the bottom diagram has been computed using the population synthesis models by Buzzoni (1995). The dashed line shows the locus of the main sequence for galactic stars. The circles on the line have an area proportional to the expected fraction of stars as computed with the Robin et al. (1995) model of the galaxy, on which basis a total of ~ 60 stars should be present between $r = 20.5$ and the completeness limit.

(along the dashed line in Fig. 3 which shows the locus of main sequence stars).

At the left of the $c-m$ relation (Fig. 2) we observe a handful of blue objects which we believe disk galaxies belonging to the cluster. These are in limited number in agreement with the cluster morphology, Bautz-Morgan I, which calls for a population dominated by early type galaxies. Always in agreement with the cluster morphology, these galaxies are located in the cluster outskirts and their density peaks at about 500 arcsecs from the cluster center or at about 1 core radius.

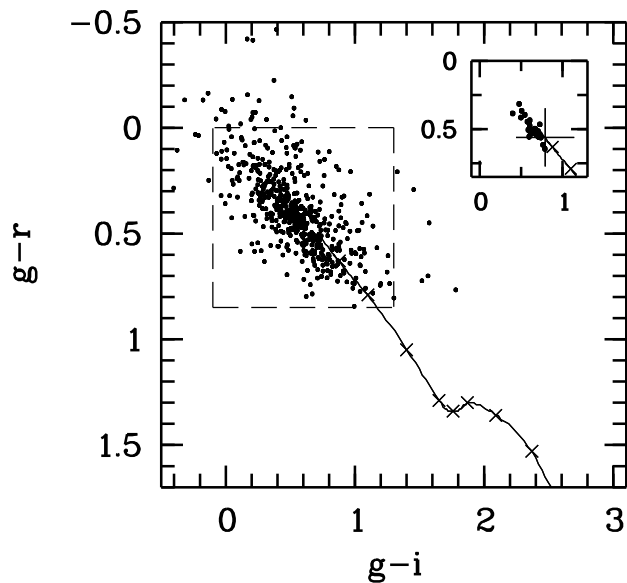


Fig. 4. The $g-i$, $g-r$ plot for the fiducial early type galaxies as identified in the $c-r$ sequence. The solid line is the same photometric model (Buzzoni 1995) as in Fig 3 and the ticks mark every 0.1 in z . The inset panel plots the dashed region selecting only the bright ($r < 18$) galaxies showing a narrower distribution. With negligible poissonian errors the colour dependence on the magnitude is the only source of (intrinsic) scatter. On the place of modelled colours for a $z = 0.03$ galaxy, the big cross closely matches the brightest galaxies in our sample.

3.2. The early type galaxies

Their distribution in the colour-colour plot, Fig. 4, match what we would expect for an ensemble of early type galaxies at the cluster redshift. The morphological type and the colour-magnitude sequence allowed us to define a subsample of E/S0 galaxies that quite likely are cluster members, indeed the main component of the cluster. The cluster of points in the plot is rather scattered. This is due to two effects: 1) an intrinsic scatter in the colour of elliptical galaxies mainly due to the correlation between absolute magnitude and colour and 2) measuring errors in the colour of the faintest galaxies. For comparison and clarity we inserted in Fig. 4 the colour-colour plot for the cD and for the galaxies with $r < 18$ magnitude. The large

cross marks the expected position a very bright elliptical galaxy would have in this diagram at the cluster redshift. As expected due to the cleaner sample and to the more accurate magnitudes of the bright galaxy colours, the plot presents a much smaller scatter.

Granted that the early type galaxies better define the cluster and seem to be, at least in the central part, the cluster itself, we look at their spatial distribution. This is not fit by a single King profile and in fact we can not define a regularly decreasing density function by using only these galaxies. At about 1 to 1.5 core radii we detect a rather well defined substructure. To check for luminosity segregation we choose to restrict the analysis for the brightest E/S0 ($r < 20$) finding a quite regular cluster density distribution with a core radius $R_c = 242 \text{ h}^{-1} \text{ Kpc}$ ($h = H_0/100 \text{ km/sec/Mpc}$). Also morphological segregation can be quantified by looking at the density profile of all (not only E/S0) galaxies brighter than $R = 20$. The R_c become larger, as expected, to an extent of $R_c = 330 \text{ h}^{-1} \text{ Kpc}$.

4. THE LUMINOSITY FUNCTION

The best way to subtract the background is to subtract a control sample obtained with the same instrumentation used for the object sample. That is why we selected to observe the cluster also at large distances from the cluster center. The furthestmost frame of our sample is located at about $r = 2.5$ cluster radii using $R_c = 242 \text{ h}^{-1} \text{ Kpc}$. Assuming a King profile distribution, this is quite reasonable for the scope, we expect that in this frame the density of cluster galaxies is less than about $1/12$ the density we have in the central region of the cluster. The outskirts region is, for our purpose, quite suitable for background number counts correction. In fact our counts in the outskirts of the cluster are in excellent agreement with Tyson (1988 and references therein). In any case our method of subtraction of two nearby (in fact neighbouring) areas will eliminate some contribution of pure cluster population but, at the same time, overcomes at best the problem of cosmic variance in background numbers counts which acts as major error source at the faint end of LF (Trentham 1997). In our analysis we cannot and will not take into account such variance as error in background subtraction, considered as affected by counting statistics only. Figure 5 is quite illustrative of the work we are doing. Here we plot our rough counts, that is before detailed processing as a function of the distance from the cluster center, as a function of magnitude superimposed to the counts by Tyson. The incompleteness correction technique described in section 2 can give a very limited help in the number counts measurements. It only affects seriously the very faint magnitudes ($r > 23$) even if the contribution of the hiding cD halo is taken into account (see the dashed line in the faint magnitude bins in Fig. 5). We clearly evidence the main features of the sample: 1) the bump at the bright magnitudes as

due to the presence of the cluster core, 2) over the whole field the cluster is easily washed out at $r \sim 20$ when compared to absolute counts and 3) from about $r \sim 22$ to $r \sim 24$ magnitude we evidence the incompleteness of our sample. Obviously this does not affect our work because we took that into account in two different ways: a) we estimated the incompleteness by simulation as mentioned in Section 2 and detailed in the paper by Moretti et al. (1998) and b) we chose to use only our frames for subtractions so that the limiting magnitude of the two operand is exactly the same and the background population are as close as possible.

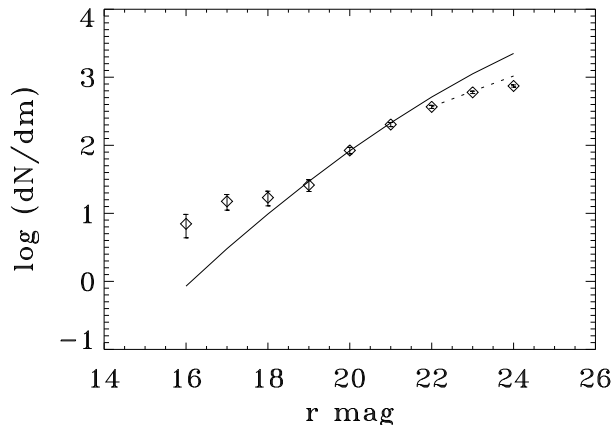


Fig. 5. Comparison between Tyson (1988) number counts (solid line). A496 counts are plotted with poisson error bars. It is easy to recognise the overdensity due to the cluster presence at bright magnitudes and the incompleteness of our observations that starts after $m \sim 22$. The dashed line represents the correction to our counts for the incompleteness due to crowding and background level differences due to cD presence. The correction is based on a bootstrap technique as described in section 2 and only affects significantly magnitude bins $r > 23$.

The complete cluster luminosity function, that is using all galaxies independently of their colour or morphological type, is simply determined as the difference between the total distribution in magnitudes and that related to the background. Obviously the maximum contrast between cluster and background is obtained by using the central field for the cluster and the outermost field for the background. The luminosity function so derived is illustrated in Figure 6 in the three different colours in which we observe.

4.1. The Composite Luminosity Function of A496

It is clear that in all colours we observe, Figure 6, a minimum in the distribution about the magnitude $m \sim 19$ which corresponds to a net separation between the distribution of giant normal galaxies and dwarfs. This is very

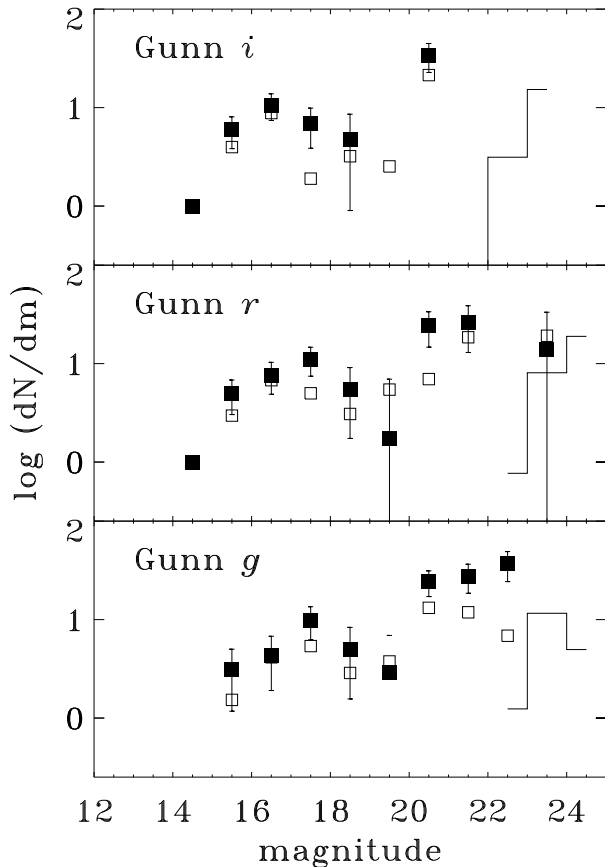


Fig. 6. Luminosity function in the filters g , r and i for the central region of A496. The error bars have been computed using poisson statistics. Filled squares to galaxies within 600 arcsec from the centre (without error bars to avoid confusion) while open squares refer to galaxies within 300 arcsec. All the objects which were not classified as bright stars ($r < 20.5$ as described in section 2) are used for the analysis: the distribution within 600 (or 300) arcsec from cluster centre are corrected subtracting the distribution of the outer frame properly normalized. The histogram at faint magnitudes in each panel shows the statistically expected losses of objects due to the presence of the cD halo.

similar to the result obtained by Biviano et al. (1995), albeit much more robust because of the more net separation, the three colours and the higher statistics. As we are dealing with bright objects no sensible effect due to the choice of our isophotal magnitude is expected.

We must point out, however, that Biviano et al. were able to evidence the effect because of the very clean selection of cluster members due to the fact that for the Coma galaxies a large number of redshifts is available. That is important because it means that the detected effect is not so evident in Coma using counts alone and that is demonstrated by the work by Bernstein et al. (1995).

To some extent we can say that such a result was implicit in the Virgo cluster works by Binggeli et al.

(1988), which could identify morphological types of galaxies, (1988) and Capaccioli et al. (1992), which found two distinct population among the early type and spiral bulges in the fundamental plane.

We then take into consideration the subset defined by the fiducial early-type galaxies that follows the colour-magnitude relation, as shown in Fig 2. This sample is quite reasonably composed by member galaxies and constitutes the major component of the cluster population, as discussed in section 3.2. Binned counts are shown in Figs. 7, 8, 9 with poisson errors. The way to fit the observed counts is self-evident looking at the distribution. We have chosen to fit it by using a gaussian plus a Schechter function. Other functions (e.g. Erlang) might obtain a better fit, but it is not clear however what that would physically mean. Given the small difference we prefer, at this time, not to look into more details. We used a maximum likelihood method exploring a 5-dimension grid of parameters defined by the function:

$$\frac{dN}{dm} = \phi \{S(\alpha, m_*) + \rho G(m_0, \sigma)\}$$

where

$$S(\alpha, m_*) = 10^{-0.4(m-m_*)(\alpha+1)} e^{-10^{-0.4(m-m_*)}}$$

and

$$G(m_0, \sigma) = e^{-(m-m_0)^2/2\sigma^2}$$

The normalization factor ϕ is computed integrating the number of objects that have $r \leq 23$. Here we stop the computation of LF due to the incompleteness of the g - r colour distribution at these magnitudes. The parameter ρ modulates the ratio between the gaussian distribution and the Schechter function. In Table 1 we report the results and the 1 sigma confidence interval for the 5 parameters α , m_* , m_0 , σ and ρ .

In every filter the case of a null contribution from the gaussian function is excluded at a very high confidence level ($> 3\sigma$). Its value, however, differs in different colours and this is mainly due to the limited statistics and fitting procedure. That will be improved with other cluster estimates as soon as the data analysis will be completed.

This is an important result and definitely indicates a bimodal distribution for the cluster luminosity function. Indeed now that we have these results we can look at the sequence which goes from the irregular to regular clusters, from Bautz-Morgan type III to Bautz-Morgan Type I. We can rely only on three clusters: Virgo, Coma and A496. The indication is clear however. In the very irregular Virgo cluster the E/S0 contribution to the luminosity function is not so dominant and it is hardly noticeable in the composite luminosity function. The gaussian peak magnitude is at $b_T = 13.0$, equivalent to $M_i \sim -20.5$ (Binggeli et al, 1988, also report of a scarce but similarly bright component of E/S0 in the field).

The bump is noticed at the same $M_i \sim -20.5$ in the clean sample selected by Biviano in the Coma cluster. This is not so evident, however, in the counts used by Bernstein et al. (1995) even if a plateau could be guessed. On the contrary it is clear and sound in A496, peaking at $M_i \sim -20$. Accordingly the evidence of the lack of galaxies on the right of the gaussian peak becomes more evident.

On the basis of these preliminary indications we thus expect that the contribution of the bright gaussian increases with the cluster morphological type, from irregular to relaxed shapes. Again this is a major result having very strong implication in the formation and evolution of clusters and which we will further test with the analysis which is still in progress.

The faint end of our A496 luminosity function is slowly rising with a slope parameter $\alpha \sim 1.65$ for the r band. The effect on the steepness of a different magnitude definition is visible in Figs. 7,8 and 9 marked with open squares. The α parameter increases up to $\alpha \geq 2.0$ for the same r band. Similar conclusions can be obtained for all the filters.

5. Summary and Conclusions

We have discussed the catalogue listed in Moretti et al (1998). The catalogue is the result of measuring about 2000 objects in 4 frames and in three (g , r and i) colours. The major result of this work is that we established that in the cD cluster A496 the luminosity function is bimodal with the early type population clearly fitted by a gaussian distribution while the dwarf galaxies obey a Schechter function with a rather high slope on the faint end. With an absolute magnitude of $M_r \sim -18.5$ we find the gap 1 mag fainter than previously observed in Coma (Biviano et al. 1995) The indication is that the amplitude of the gaussian respect to the Schechter function depends on the cluster morphology, going from a barely noticeable gap in irregular clusters (e.g. Virgo) to a clear evidence in evolved clusters (Bautz-Morgan type I).

The somewhat high slope in the dwarf domain, with $\alpha \sim 1.65$ does not differ too much from other authors findings in similar clusters (Trentham 1997, 1998). While it is not possible to compute the value of α at $M_r = -20$ because of the gaussian shape of the LF in the bright end, the comparison between our result and their work give a higher slope for A496. Taking into consideration the discussed correction for the magnitudes we even reach the very steep value of $\alpha \sim -2.0$, close to the value reported by De Propris et al (1995) for the dwarves in A665. This thesis will be fully developed in the work that is continuing with the complete photometry for the 19 selected clusters.

References

- Bernstein, G.M., Nichol, R.C., Tyson, J.A., Ulmer, M.P., Wittman, D., 1995, AJ 110, 1507
 Binggeli, B., Sandage, A., Tamman, G.A., 1988, ARA&A 26, 509

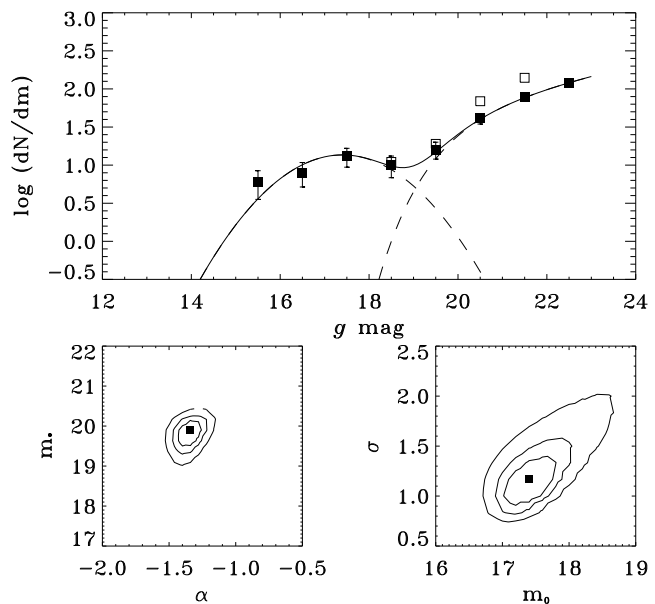


Fig. 7. Luminosity function in the filter g for the early type galaxies, as selected in the colour-magnitude plane of Fig. 2. A magnitude cut-off was set to $r = 23.0$ to avoid the incompleteness in the g passband. This selection made the subsample used for early type galaxies LF determination 90% (or higher) complete in all three filters. The points (and poissonian error bars) are built from a 1 mag binning and are shown for comparison with the function derived from maximum likelihood methods. The dashed lines are the gaussian (leftmost) and Schechter (rightmost) separated distribution which contribute to the sum (solid line). For completeness we added, shown as open squares, the LF with the corrected magnitudes (see section 2): the steepness of the faint end increases as expected. The lower panels shows 1σ , 2σ and 3σ confidence intervals for the composite function parameters, computed with the uncorrected isophotal magnitudes.

Table 1. A496 LF parametrization for the g , r and i filters.

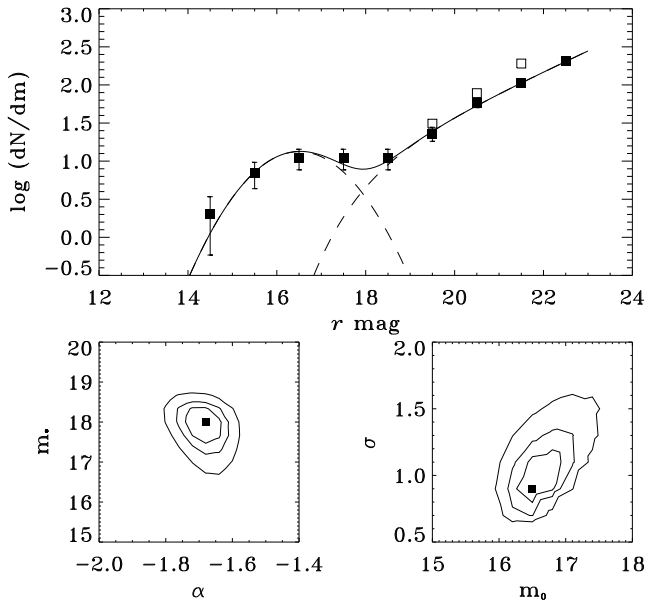
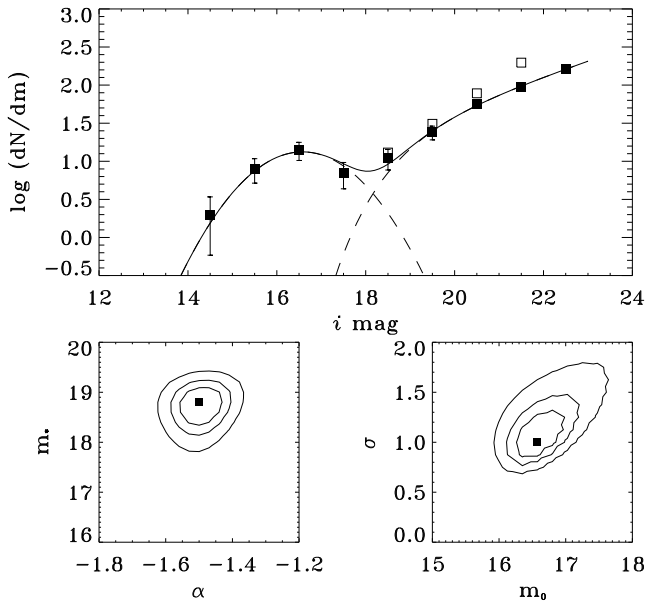
	α	m_*	m_0	σ	ρ
g	$-1.34^{+0.06}_{-0.04}$	19.8^{+2}_{-2}	17.4^{+2}_{-2}	$1.10^{+0.17}_{-0.13}$	$0.22^{+0.04}_{-0.04}$
r	$-1.69^{+0.04}_{-0.04}$	18.0^{+3}_{-3}	16.5^{+2}_{-2}	$3.5^{+0.00}_{-0.20}$	$1.07^{+0.18}_{-0.20}$
i	$-1.49^{+0.04}_{-0.04}$	$16.0^{+3.0}_{-0}$	16.6^{+2}_{-2}	$1.04^{+0.16}_{-0.12}$	$0.44^{+0.09}_{-0.08}$

Errors quote 1σ confidence intervals

- Biviano, A., Durret, F., Gerbal, D., Le Fevre, O., Lobo, C., Mazure, A., Slezak, E., 1995, A&A 297, 610
 Buzzoni, A. 1995, ApJS 98, 69
 Capaccioli, M., Caon, N., D'Onofrio, M., 1992, MNRAS 259, 323
 Colless, M., 1989, MNRAS 237, 799
 De Grandi, S., 1996, PhD Thesis, Università di Milano
 De Propris, R., Pritchet, C.J., Harris, W.E., McClure, R.D., 1995, ApJ 450, 534
 De Propris, R., Pritchet, C.J., 1998, astrp-ph/9805281
 Lopez, O., Yee, H.K.C., 1996, in: proceedings of "Fresh Views of Elliptical Galaxies", Eds. A.Buzzoni, A.Renzini, A.Serrano (ASP: San Francisco) p.279

Tyson, J.A., 1988, AJ 96, 1

West, R.M., Kruszewski, A., 1981, Ir. Astr. J. 15, 25

Fig. 8. Luminosity function in the filter r . Same as Fig. 7.Fig. 9. Luminosity function in the filter i . Same as Fig. 7.

Marzke, R.O., Huchra, J.P., Geller, M.J., 1994, ApJ 428, 43
 Metcalfe, N., Godwin, J.G., Peach, J.V., 1994, MNRAS 267, 431

Molinari, E, Smareglia, R., 1998, A&A 330, 447

Moretti, A., Chincarini, G., Molinari, E., De Grandi, S., 1998, in preparation

Robin, A., Haywood, M., Gazelle, F., Bienaymé, O., Crézé, M., Oblak, E., Guglielmo, F., 1995, http://WWW.obs-besancon.fr/www/modele/modele_ang.html

Secker, J., 1996, ApJ 469, L81

Trentham, N., 1997, MNRAS 290, 334

Trentham, N., 1998, MNRAS 294, 193

This article was processed by the author using Springer-Verlag L^AT_EX A&A style file L-AA version 3.